Results in Engineering 27 (2025) 106932

Contents lists available at ScienceDirect

Results in Engineering

journal homepage: www.sciencedirect.com/journal/results-in-engineering

Research paper

Scaling turbulent wake flow downstream of isolated piers in laboratory and river

Massimo Guerrero [a,*], Rui Aleixo [b], Leonardo Schippa [c]

[a] Department of Civil, Chemical Environmental and Materials Engineering, University of Bologna, Bologna, Italy
[b] Institute of Hydro-Engineering of the Polish Academy of Sciences, Gdansk, Poland
[c] Hydraulics Engineering Department, University of Ferrara, Ferrara, Italy

A R T I C L E I N F O

Keywords:
Bridge pier wake
Turbulence
Experimental scaling
Po River
Power density spectrum
Leonardo da Vinci

A B S T R A C T

The flow around a bridge pier is a classic example of fluid-structure interaction in hydraulics where different phenomena coexist, namely: contraction of the flow section, vortex ejection, generation of horse-shoe vortexes and possible bed erosion. Knowing how the fluid and pier interact, and the role of the generated turbulent wake is crucial for the design of stable bridges and riverbeds. Physical modelling in the laboratory together with numerical modelling are two important tools to address the study of the flow around the bridge pier. Results from physical modelling in reduced scale models must be transferred to prototype obeying similarity criteria defined by the appropriate non-dimensional parameters such as Reynolds and Froude numbers.

This paper presents an investigation on scaling turbulent wake flows downstream of isolated piers based on the ratio between the water level drop and the obstacle's flow facing width. Turbulent flow measurements were carried out both on scale models of different geometries of bridge piers in the hydraulics laboratory and around a real bridge pier at the Po River in Italy.

The proposed scaling is applied to Leonardo da Vinci's drawings of turbulent flow past a vertical obstacle aiming at providing insights and quantitative information about his drawings.

1. Introduction

Although analytical solutions for the Navier-Stokes equations exist [1–3], these are limited to a few cases, frequently dominated by viscosity. For most fluid mechanics problems, in particular environmental flows often characterized by large Reynolds numbers (turbulent flows) and complex geometries, it is not possible to derive an analytical solution of the Navier-Stokes equations [4]. For example, when dealing with river flows, the Reynolds number of such flows is typically in the range of 10^6 – 10^9 leading to a relevant contribution of inertial forces due to turbulent vortices. This requires solving the oscillating components of water velocity with a time resolution that is orders of magnitude higher than for mean flow dynamics. This misalignment between the resolution needed to describe turbulent water oscillations and river mean flow dynamics yields to simplified mathematical modelling that requires well educated calibration procedure entailing experimental datasets [5,6].

The flow around an isolated bridge pier is an example of a flow without an analytical solution but that can be analyzed by means of experimental and numerical methods. Experiments carried in laboratory under controlled conditions are crucial for a better understanding of the different fluid mechanics phenomena induced by the flow-bridge pier interaction (Dargahi1998, [7–10]). However, the results of these experiment have to be properly scaled to the prototype to be built. To the authors best knowledge, a relevant gap in scientific literature is about how to properly scale turbulent flow around piers when passing from laboratory results to actual bridge piers size. Therefore, in this study we focused on scaling criteria for turbulent flow downstream of isolated piers useful for physical modeling of bridge piers in hydraulic engineering practice. Scaling turbulent flow around piers to fit laboratory typical conditions is a relevant engineering practice that is challenged by the actual possibility of fulfilling the same values of different non-dimensional parameters. The impossibility of reproducing all those parameters at the same time introduces biases in physical modeling, referred as scale effects [11].

The criterion for accurately reproducing turbulent fluctuations was investigated by comparing a real bridge pier (prototype) at the lower reach of the Po River in Italy with laboratory scaled models of bridge piers. In all cases, turbulent fluctuations were assessed by means of ultrasound techniques which provided power density spectrum of those

* Corresponding author.
E-mail addresses: massimo.guerrero@unibo.it (M. Guerrero), rui.aleixo@ibwpan.gda.pl (R. Aleixo), leonardo.schippa@unife.it (L. Schippa).

https://doi.org/10.1016/j.rineng.2025.106932
Received 28 May 2025; Received in revised form 14 August 2025; Accepted 25 August 2025
Available online 25 August 2025

List of symbols

C_r	Pier resistance coefficient
D	Pier model width
$dy = y - y_{wk}$	Water level drop across pier
$\varepsilon = UD$	Turbulent viscosity representing the horizontal diffusion
f	Vortex sheading frequency
$Fr = \frac{U}{\sqrt{gy}}$	Froude number immediately upstream the pier
$Fr_{wk} = \frac{U_{wk}}{\sqrt{gy_{wk}}}$	Froude number at pier wake
g	Gravitational acceleration
h	Water depth
L	Flow length scale
ν	Water kinematic viscosity
PSD	Power spectra density of velocity oscillation
$Re = \frac{Uy}{\nu}$	Reynolds number immediately upstream the pier
$Re_{wk} = \frac{U_{wk}y_{wk}}{\nu}$	Reynolds number at pier wake
$Re(D) = \frac{UD}{\nu}$	Pier Reynolds dimensionless parameter
ρ	Water density
Sh	Shields dimensionless parameter
St	Strouhal dimensionless parameter
$S_{vh} = \frac{dy}{D}$	Geometrical dimensionless parameter: vertical to horizontal scaling
u'	Velocity oscillation around time averaged velocity
U	Flow velocity immediately upstream the pier
U_{wk}	Flow velocity at pier wake
UVP_b	UVP probe measuring velocity vertical component from the bottom
UVP_p	UVP probe encased within the pier model and measuring 30° inclined velocity component
UVP_{wk5}	UVP probe measuring velocity vertical component within the pier wake 5 cm downstream from it
UVP_{wk10}	UVP probe measuring velocity vertical component within the pier wake 10 cm downstream from it
UVP_{wk15}	UVP probe measuring velocity vertical component within the pier wake 15 cm downstream from it
y	Water level immediately upstream the pier
y_{wk}	Water level at pier wake

fluctuations. This comparison was built on known scaling criteria, namely the Reynolds, Froude and Strouhal dimensionless parameters and provided novel insights about the scaling of turbulence with the pier width and water level drop across it. The ratio defined by the pier width and water level drop, represented well the three-dimensional feature of boundary layer separation around a vertical pier, namely the horseshoe vortex [12].

1.1. Scaled models in fluid mechanics

Scaling prototypes into laboratory facility size models is a consolidated approach in fluid mechanics to investigate fluid flowing under controlled conditions [13,14]. Since Osborne Reynolds studies [15] to determine flow resistance in pipes, the experimental approach has been a proficient method to develop our knowledge about fluid mechanics. Particularly relevant to the experimental approach, the Vaschy-Buckingham theorem [16,17] provides dimensionless groups of variables involved in the physical process under investigation. Indeed, the mathematical equations describing physical phenomena are frequently reported in their dimensionless form that yields a broader meaning of the described dynamics not depending on the specific study case size. For the experimental approach, this entails the following: i) fixing relevant variables describing the investigated process, ii) applying dimensional analysis, iii) deriving non-dimensional groups, and finally iv) assessing those variables scaling for non-dimensional groups unchanged when passing from model to prototype size. Theoretically speaking, similar processes might be reproduced at different scales provided that dimensionless groups keep the same values for the different scales tested. Practical applications regard any hydraulic scale models where prototypes are reproduced at smaller size to test their performance under controlled conditions while targeting at validating the final design before construction [14,18,19].

In practice, few non-dimensional groups keep the same values when passing from prototype to scale model size whereas others are disregarded. In fact, the Buckingham theorem usually determines many dimensionless groups for the investigated dynamics which would yield over definition of model scale. This makes experimental hydraulics particularly challenging as it relies heavily on expert judgment in selecting the most relevant dimensionless groups.

Depending on the application, specific dimensionless groups are applied in fluid mechanics, for example, to keep the ratio between (i) inertial and viscous forces, i.e., the Reynolds number (Eq. (1.1)), (ii) inertial and mass forces, i.e., the Froude number (Eq. (1.2)), (iii) local and convective accelerations, i.e., the Strouhal number (Eq. (1.3)), (iv) bottom shear stress and submerged mass force of loose sediment forming the riverbed, i.e., the Shields number (Eq. (1.4))

$$Re = \frac{UL}{\nu} \tag{1.1}$$

$$Fr = \frac{U}{\sqrt{gh}} \tag{1.2}$$

$$St = \frac{fL}{U} \tag{1.3}$$

$$Sh = \frac{\tau_0}{(\rho_s - \rho)gd_{50}} \tag{1.4}$$

where U is the scale of the flow velocity, L is the relevant length size of the flow domain, h is the flow depth, f is the frequency of flow vortex shedding, ρ and ν are the fluid density and kinematic viscosity (10^3 kg/m^3 and 10^{-6} m^2/s for water at 20 °C, respectively), τ_0 is the shear stress at river bottom operating on loose sediment having median diameter d_{50} and density ρ_s, and g is the acceleration due to gravity. Often, when scaling models, it is not possible to respect every dimensionless parameter. For example, fixing the protype ratio between inertial and viscous forces, the Reynolds number yields an inverse proportionality between model size and scaled flow velocity in the model, i.e., smaller length size means larger flow velocity for the model than for prototype if water viscosity is unchanged. Passing to Froude number, for the same example, the flow depth is certainly related to flow domain size (e.g., the flow depth to width ratio) that, for given prototype ratio between inertial and mass forces and unchanged gravity, yields a direct proportionality between model size and scaled flow velocity which contradicts Reynolds number criteria of scaling. Something similar might be argued by analyzing the Strouhal number, i.e., model size and scaled flow velocity should proportionally change when passing from prototype to model, although this direct proportionality differs from Froude number criteria of scaling for example because of the effect of possible change in frequency vortex shading when passing from prototype to model.

2. Methodology

2.1. Isolated pier laboratory experiments

A set of experiments were conducted in the recirculating hydraulic flume of the University of Bologna. This flume is 14 m long, 0.5 m wide and 0.7 m heigh. The flume had side glass walls allowing for optical access to the flow and it was slightly sloped towards the outlet ($i = 0.13$ %). Its bottom had a paint coating so that it could be considered smooth. The water level ranged from 0.11 m to 0.22 m just upstream of the tested pier whereas the flume Reynolds number was fixed to about 8.0×10^4. The obstacle was placed at 8.5 m of the inlet where the turbulent boundary layer was likely extending to the entire water depth for all tests.

Rectangular, semicircular and triangular (isosceles) prisms were vertically mounted on the flume bed at its central line (Fig. 1a) to model different isolated piers. The rectangular prisms base was 5 cm width by 10 cm long and 2.5 cm width by 5 cm long (Configurations R and R5), the half-circle prism base had 10 cm diameter (Configuration C), and the isosceles triangle had a base of 10 cm (Configuration T). The different prisms are depicted in Fig. 1b For each configuration, two flow rates were tested.

Table 1 summarizes the different variables tested for each configuration where D is the pier model width, y and y_{wk} are water levels immediately upstream of pier and at pier wake, $dy = y - y_{wk}$ is the difference between the water levels, S_{vh} is ratio defined by the pier width and water level drop across pier, U and U_{wk} are flow velocities immediately upstream and at pier wake, the pier Reynolds number $Re(D)$ and Froude numbers are assessed with Eqs. (1.1) and 1.2 respectively by adopting variables immediately upstream of pier or at pier wake the latter where indicated by subscript *wk*.

The ratio between water level drop and cylinder width, hereafter referred as vertical to horizontal saling parameter defined as $S_{vh} = dy/D$ is here introduced. Increasing S_{vh} values also reflect the complexity of turbulent flow field around a cylinder. This typically develops into flow separation downstream of the cylinder, three-dimensional vortex structures (namely the horseshoe vortex) and downstream vortex shedding. This three-dimensional complexity derives from the upstream boundary layer overcoming the gradient pressure imposed by the obstacle. This differs from simpler two-dimensional vortex structures as it is described in the experimental work of Dargahi [12]. The proposed S_{vh} dimensionless parameter represents the three-dimensional features of vortex structures in conducted experiments. Higher S_{vh} means relative greater pressure drop faced by the upstream boundary layer and therefore more complex turbulent flow structures at the obstacle's wake.

2.1.1. Velocity measurements in the scaled model

An Ultrasonic Velocity profiler (UVP) was used to measure the velocity profiles at different sections with high spatial and time resolutions. The UVP, first proposed by Takeda [20,21] is nowadays an established technique that works based on the acoustic Doppler effect. This technique is implemented in instruments produced by different manufacturers and has been successfully deployed in a wide range of applications since the nineties of last century (e.g., [20,22–25]).

A UVP probe measures time and spatial independent instantaneous profiles of the flow velocity component aligned to the ultrasound beam with an acquisition frequency up to few hundred Hz. The Doppler shift detection and beam range gating are determined resulting in a time and spatial resolved velocity profile [21].

The single-component UVP by Signal Processing ([26], Model 2125, User's manual) was used with time and spatial resolutions in the ranges of [5 ms, 10 ms] and [0.5 mm, 1.1 mm] respectively.

Five 4 MHz and 8 mm diameters UVP probes were measuring the

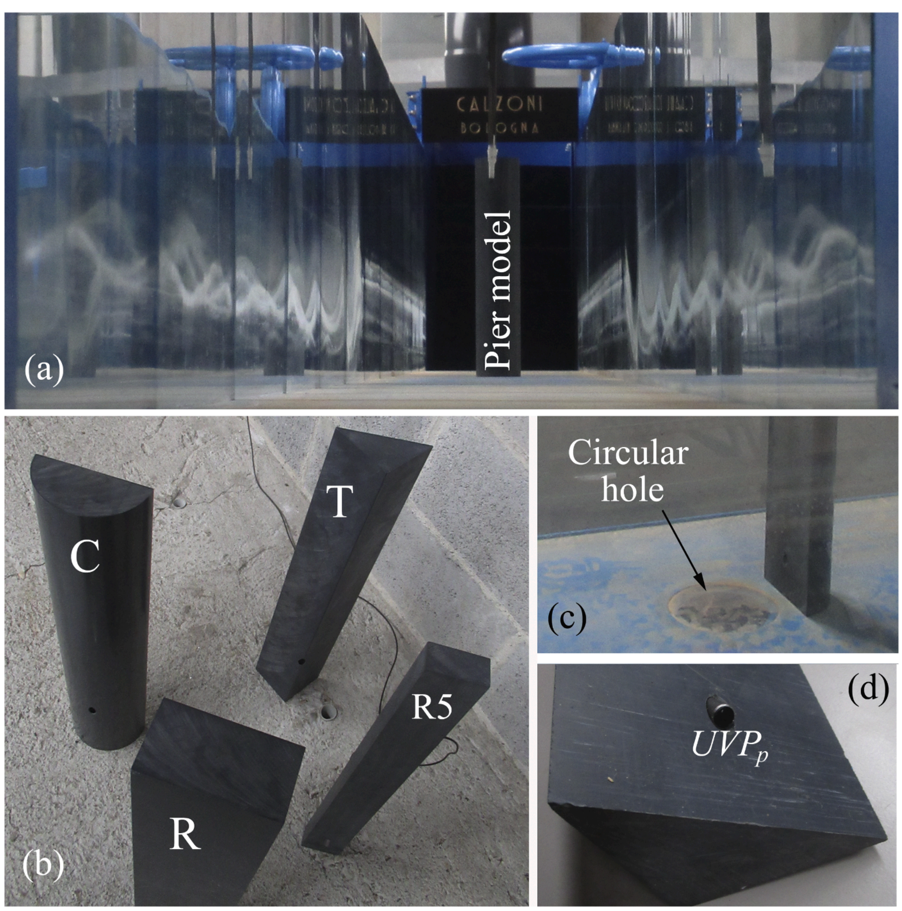

Fig. 1. (a) Pier model within the side glass bounded flume of University of Bologna framed from the outflow section. (b) Tested prisms. (c) Wake region with the hole at flume bottom for UVP deployment. (d) UVP pit protruding from the downstream oriented face of triangular prism.

Table 1
The different configurations tested in the hydraulic flume at University of Bologna. Configuration R and R5 rectangular prism with $D = 0.1$ m and $D = 0.05$ m respectively, Configuration C: half circle, Configuration T: isosceles triangle. Corresponding features for the investigated pier bridge at Po River (Italy).

Low flow condition (40 l/s)									
Configuration	D (m)	U (m/s)	U_{wk} (m/s)	y (m)	y_{wk} (m)	Fr (-)	Fr_{wk} (-)	$S_{vh} = dy/D$ (-)	$Re(D)$ (-)
R	0.1	0.57	1.60	0.140	0.050	0.49	2.28	0.90	5.7E+04
R5	0.05	0.73	1.51	0.110	0.053	0.70	2.09	1.14	3.6E+04
C	0.1	0.63	1.60	0.128	0.050	0.56	2.28	0.78	6.3E+04
T	0.1	0.61	1.63	0.132	0.049	0.53	2.35	0.83	6.1E+04
High flow condition (80 l/s)									
Configuration	D (m)	U (m/s)	U_{wk} (m/s)	y (m)	y_{wk} (m)	Fr (-)	Fr_{wk} (-)	$S_{vh} = dy/D$ (-)	$Re(D)$ (-)
R	0.1	0.37	1.07	0.215	0.075	0.26	1.24	1.40	3.7E+04
R5	0.05	0.43	0.78	0.185	0.102	0.32	0.78	1.66	2.2E+04
C	0.1	0.40	0.93	0.200	0.086	0.29	1.01	1.14	4.0E+04
T	0.1	0.39	1.11	0.207	0.072	0.27	1.32	1.35	3.9E+04

Bridge pier at Po River						
	D (m)	U_{wk} (m/s)	y_{wk} (m)	Fr_{wk} (-)	$S_{vh} = dy/D$ (-)	$Re(D)$ (-)
South position	3.0	1.0	5.7	0.13	0.03	5.7E+06

profiles of the velocity in different sections; namely: UVP_b, UVP_p, UVP_{wk5}, UVP_{wk10} and UVP_{wk15} as indicated in Fig. 1.

The bottom UVP_b accomplished non-intrusive profiling of the vertical component of velocity. In this case, a circular hole was drilled in the flume bed. A flat plate made of polymethyl methacrylate (PMMA) was placed to cover the hole (Fig. 1c), flush mounted with the channel bed to minimize the perturbation. In this plate, the UVP_b probe was placed looking up, allowing for non-intrusive measurements of the velocity vertical component at 5 cm downstream from the obstacle. In addition, the same probe was also used to infer the water surface position. This was assessed by detecting the maximal echo intensity along the profile, with 1.1 mm spatial resolution, in all laboratory tests including two free flow conditions in the absence of pier models. This maximal intensity is due to coherent and uncoherent reflections at the interface between media characterized with very different acoustic impedances [27] such as air and water interfaces.

The UVP_p at the pier was measuring a 30° to vertical slant component which was mostly affected by the velocity oscillation in the flow direction. This probe was completely encased in the pier model. The probe pit was protruding for a maximum of 2 mm (Fig. 1d) in the turbulent wake region and placed about 6 cm above the bottom that performed a non-intrusive measurement above the flume bottom.

Additionally, three profiles of velocity vertical component were sampled at the pier wake for increasing distances from the pier, at intervals of 5 cm, by looking down deploying UVP probes from water surface (i.e., UVP_{wk5}, UVP_{wk10} and UVP_{wk15} in Fig. 2a).

2.1.2. UVP data analysis

Filtering is a common post-processing step for flow velocity data acquired with ultrasound techniques. The goal of filtering is to remove possible biases due to randomness of scattering process and Doppler noise [21]. Doppler velocity data filtering is based on defined thresholding techniques such as for example phase-space thresholding [28] that is used for pointwise velocity measurement using an Acoustic Doppler Velocimetry – ADV. In this paper, filtering of velocity time series was based on Gaussian normal distribution which defines the

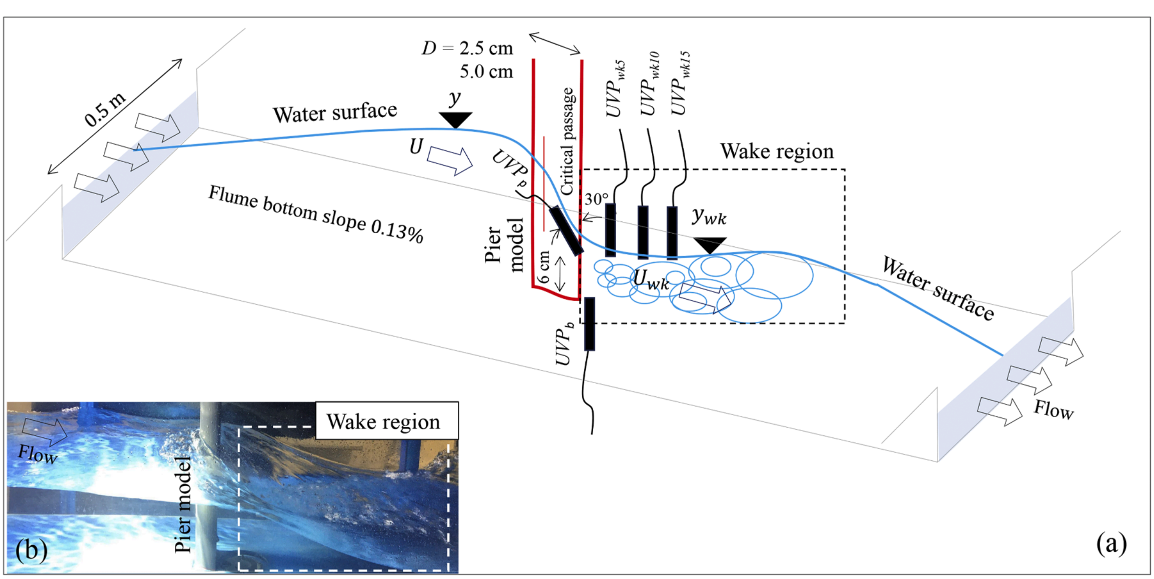

Fig. 2. (a) Pier experimental layout showing UVP probes deployment within the wake region. (b) A picture form laboratory campaign showing three-dimensional horseshoe vortex developing around model pier.

expected standard deviation of flow velocity.

Using profiling techniques such as the UVP, yields several advantages: (i) the expected shape of profile velocity might be used as an additional phase-space dimension to filter out specific positions (i.e., cells) unfulfilling the expected time averaged shape of velocity or echo profiles, (ii) within the Rayleigh regime the scattered energy in the backward direction (backscatter) is much more relevant than in other directions [27] that means louder and clearer return for monostatic UVP technology than for ADV. Therefore, Doppler velocity profiling is more robust than point wise investigation and needs limited filtering. Acquired velocity profiles were trimmed about 0.01 m close to boundaries, i.e., the flume bottom and the water to air interface to eliminate affected cells by side lobes interference and possible bias due to reflecting targets not representing fluid flow velocity. This trimming was based on thresholding techniques applied to echo intensity profiling rather than the direct filtering of corresponding velocity profiling [29]. Cells showing echo values exceedingly >2 to 3 times the average value were discarded. In a similar way, static echo filtering was applied to get rid of cells where invariable values of echo were persistent (i.e., static) that was based on echo standard deviation [29].

In this experimental campaign, echo standard deviations lower than about ten times the corresponding average value along the profile indicated consecutive reflections of the same emission from boundaries, namely ghost echoes [21]. It is worth noting that no more than three cells per profile were finally discarded, furthermore no filtering was needed in the time domain for single cell time-series. These comprised of 32,800 samples that were therefore validated for all probes and tests.

The power spectral density, PSD, of velocity fluctuations is frequently applied in turbulent flows analysis [30,31]. This was assessed at each validated cell along UVP profiles and covering the frequency range from 1 to 100 Hz. The PSD profile average was then assessed and the maximal density located which gave the oscillating frequency for the investigated velocity component reflecting the main turbulent coherent structure oscillation. The power spectral density was also computed for the water level time-series as detected by the UVP_b which measured the water surface oscillation at the obstacle wake and for free-flowing conditions in the hydraulic flume.

The time correlation, i.e., correlation as a function of time lag, was assessed for the velocity fluctuation by combining time series from the same profile. UVP time series for different cells can be considered contemporaneous although the speed of sound (close to 1480 m/s) entails a negligible delay along the profiling distance. UVP cells are virtually independent point wise probes. The first cell close to probe tip was correlated to timeseries from consecutive cells: i.e., first cell vs. second cell, first cell vs. third cell, first cell vs fourth cell and so on up to the last available cell.: time correlation was characterized along the acoustic beam alignment (i.e., corresponding to velocity component direction) that was for increasing pair cells distance. It's worth noting that maximum of the time correlation is expected for a time lag corresponding to the eddies traveling distance between cells along the beam direction (i.e., contemporaneous and independent probes). It is then possible to obtain an estimation of the eddies' celerity along the acoustic beams given by the pair cells distance divided by the time lag corresponding to the time correlation peak.

Time correlation assessment was more robust than corresponding spatial correlation, i.e., correlation between instantaneous profiles as a function of space shift. In fact, much longer time series than instantaneous profiles were available from UVP dataset (i.e., a time series made of 32,800 samples vs. about 100 cells).

A two-dimensional correlation function was eventually reconstructed where time lag is the independent main variable and distance between cells is an additional independent variable. This identifies turbulent coherent structures and possible eddies shedding [32]: high correlation values are expected for time lag and probe distance corresponding to observed oscillations period and wavelength, respectively.

Finally, for given cells pair, the integral scale was estimated as the time lag corresponding to the lag-averaged correlation value: i.e., the time correlation integral divided by the average correlation for the inspected time-lags. The integral scale reflects the oscillating period for turbulence coherent structures within the inertial subrange [32]. Averaged values along profiles were also calculated that yielded mean integral scale and celerity for each UVP probe (i.e., along acoustic beam alignment and the corresponding velocity component).

2.2. Velocity measurements in the prototype: Po River campaign

The prototype pier selected is one of three piers belonging to the bridge connecting Pontelagoscuro to Santa Maria Maddalena, in Ferrara, Italy, whose construction dates to post-World War II. The bridge is located over a 200 m width reach, in the lower portion of the Po River (44°53′17″N, 11°36′29″E), 80 km upstream the river mouth. Po River flows in the northern part of Italy from the Cozie (Cottian) Alps and for around 651 km up to the Adriatic Sea, with a draining basin area of approximately 74,091 km^2.

The bridge pier geometry is an elongated cylinder characterized by a 3 m diameter semi-circular flow facing section and a length of 13 m. The bridge pier is 80 m apart from the nearest piers and 50 m from shore line, and thus it can be considered isolated.

An Acoustic Doppler Current Profiler – ADCP campaign was conducted on 12 December 2024 during the falling limb of a moderate flood event with a measured flowing discharge of about 1500 m^3/s. Data herein reported regards the first pier from right bank which aligns to channel thalweg (Fig. 3b and c) that is the south position in Table 1.

The ADCP is a Doppler velocity profiler combining four or more ultrasound monostatic transducers and auxiliary sensors (i.e., Compass and Global Positioning System) which yield the flow velocity profile in east, north, up referenced system. Differently from UVP, the ADCP monostatic transducers are synchronized which enables three components velocity profiling although at a lower frequency (about 1 Hz). The ADCP has been extensively applied for decades in riverine environment to investigate river flow discharge, velocity filed, turbulent coherent structures and associated sediment fluxes (e.g., [33–36]).

A 1200 kHz WorkHorse ADCP (Teledyne–RDI, Teledyne RD Instruments, Poway, California [37]) was kept steady in one upstream and three downstream positions (Fig. 3b) around the investigated bridge pier at about 1 m distance from its wall (Fig. 3d and e). These positions are depicted in Fig. 3b where the time-depth averaged velocity vectors are also visible as derived from a 6 min long time-series.

The water depth immediately at downstream of the pier was reduced to about 5.7 m by debris protecting the foundation structure. Flow Reynolds and Froude number referred to this position were equal to 5.7 $\times 10^6$ and 0.13, respectively. The pier Reynolds number referred to its 3 m width was 3×10^6 and the $S_{vh} \cong 0.13$ that is one order of magnitude lower than for laboratory experiments (Table 1).

Similarly to the laboratory campaign, the power spectral density, PSD, was assessed for the velocity fluctuation at each cell (0.25 m for ADCP profiling). Consistently with UVP deployment (Fig. 2) the vertical component from ADCP profiling was compared to UVP results. The available frequency range spanned two orders of magnitude (i.e., 10^{-2}–10° Hz), two orders of magnitude lower than PSD from UVP. This results from the inherently lower acquisition frequency of ADCP relative to UVP, being a technological constraint in the transition from broadband methods, suited to environmental monitoring, to narrowband techniques, which are more appropriate for controlled laboratory environments [38].

3. Results

3.1. Power spectral density

Fig. 4a and Fig. 4b, Fig. 4c show the pier's wake in the laboratory and in the field respectively, PSDs comparison among laboratory tests and

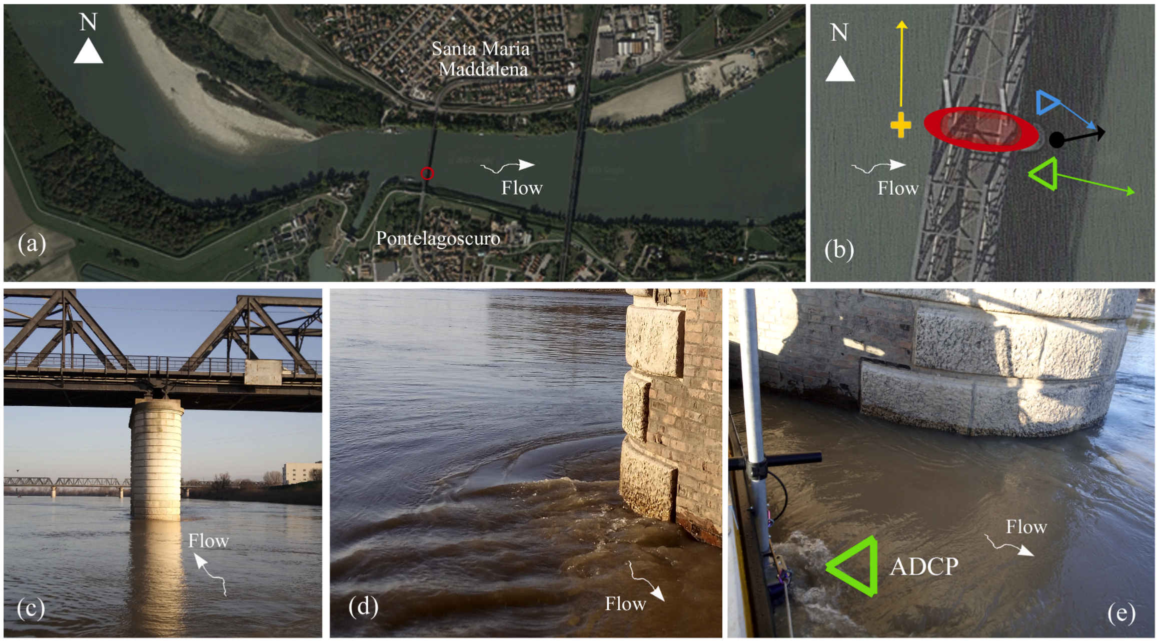

Fig. 3. (a) Po River at Pontelagoscuro (Ferrara, IT) with the investigated pier (indicated) supporting the statal road-16 bridge between Pontelagoscuro and Santa Maria Maddalena. (b) The pier viewed from above with ADCP deployment positions and time-depth averaged flow velocity vectors. (c) The investigated pier viewed while sailing upstream. (d) Details of flow wake and (e) ADCP fixed deployment (south-east position).

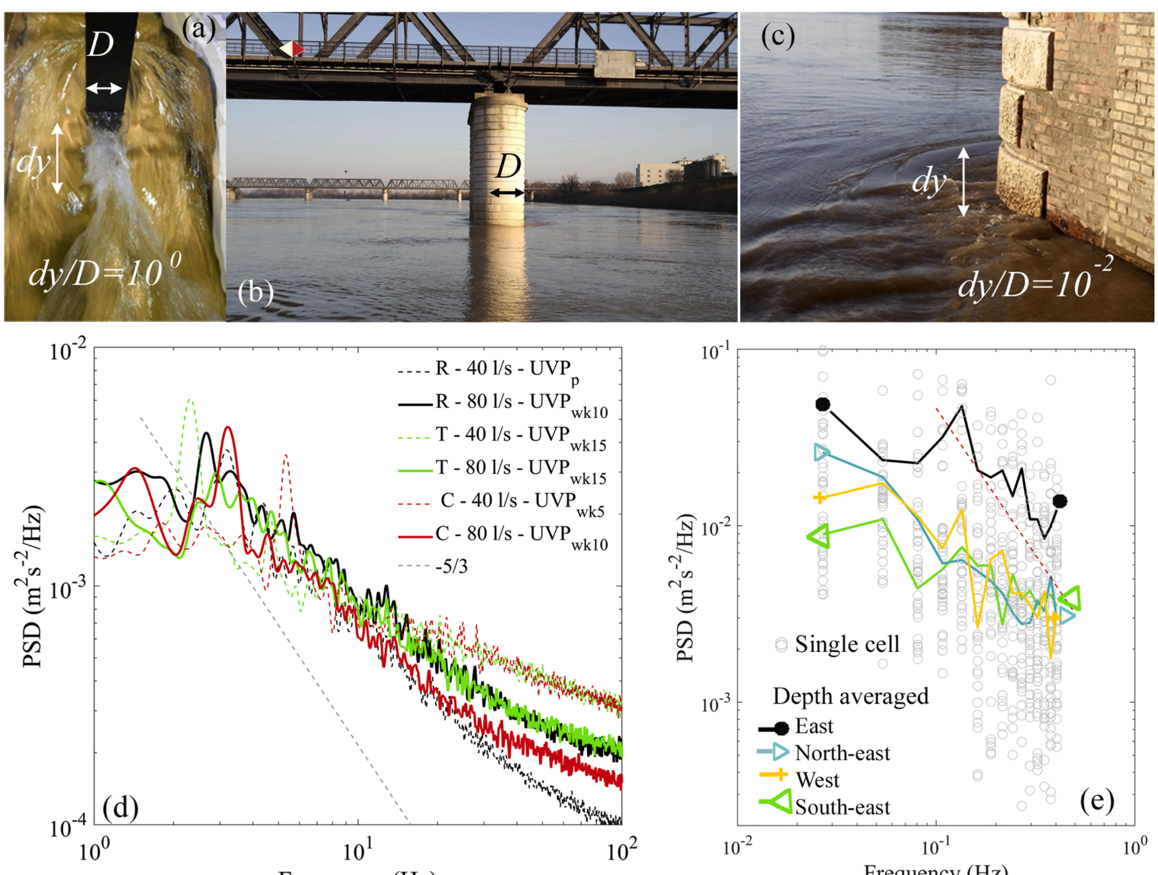

Fig. 4. (a) Horseshoe wake around pier model at the Hydraulic Laboratory. (b and c) Estimation of the dy/D ratio between water level drop and bridge pier width at the Po River. (d) PSD from UVP profiling at pier models for different configurations as reported in Table 1 and UVP probes (Fig. 2a). (e) PSD from ADCP profiling around bridge pier at the Po River for profile single cells and depth averaged at the four indicated positions in Fig. 3b.

the bridge pier is elucidated in Fig. 4d and Fig. 4e. There are significant differences between the wakes in the laboratory and in the field. The latter appears mostly laying in the water surface horizontal plane (Fig. 4b and Fig. 4c) that gave an order of magnitude lower S_{vh} dimensionless parameter when compared to laboratory piers. Although this clear difference in the vertical development of the wake observed structure, the corresponding PSDs of oscillating velocities, *u'*, appeared with similar distributions (Fig. 4d and e) although shifted towards higher frequencies for the laboratory campaign results. Peaking frequencies close to 3 to 5 Hz can be appreciated in Fig. 4d for some of the tested combinations: pier model sections, flow conditions and UVP probes. Similar peaks appeared for the bridge pier at much lower frequencies close to 0.2 Hz (Fig. 4e) that was particularly pronounced for the ADCP profiling behind the pier (i.e., East position) at wake region corresponding to UVP measurements in laboratory tests. These peaks were related to oscillating main eddies which mostly corresponded to the Strouhal dimensionless parameter [12].

Power spectral density peaks were captured also at higher frequencies for both observation scales (i.e., laboratory and prototype). These made evident the oscillation of overlaying smaller structures due to turbulence development within the inertial subrange. The resulting PSD decreasing with power −5/3 corroborated the UVP and ADCP observing of turbulent energy cascade within the inertial subrange, although energy flatten appeared for UVP measurements while approaching 100 Hz. This was likely due to unfiltered noise that in some cases might have hidden the investigated turbulence spectrum [39].

Turbulence induced noise at laboratory tests was investigated by comparing water surface oscillations downstream of tested piers and for the two corresponding free flow conditions (i.e., 40 l/s and 80 l/s) in Fig. 5.

Configurations R and R5 (Fig. 5a, b and c, d, respectively) were proficient in introducing turbulent oscillations across the entire spectrum. In fact, these sections resulted in a clearer divergence of the PSD with respect to the corresponding free flow condition, i.e., the −5/3 power law. Nevertheless, PSD peaks are visible up to 10–20 Hz for all the tested configurations.

The most protruding peaks occurred for Configuration R5 at higher flow condition (Fig. 5d) within 5–10 Hz interval. These reflected the oscillation of boundary layer separation around obstacles that was particularly evident for the small rectangular section.

Power content increased for all the tested piers when compared to corresponding free flow conditions although C and T Configurations for 80 l/s (Fig. 5f and h) presented power grouping at lower frequencies (<3 Hz).

3.2. Time correlations

Time correlations were assessed for all the configurations

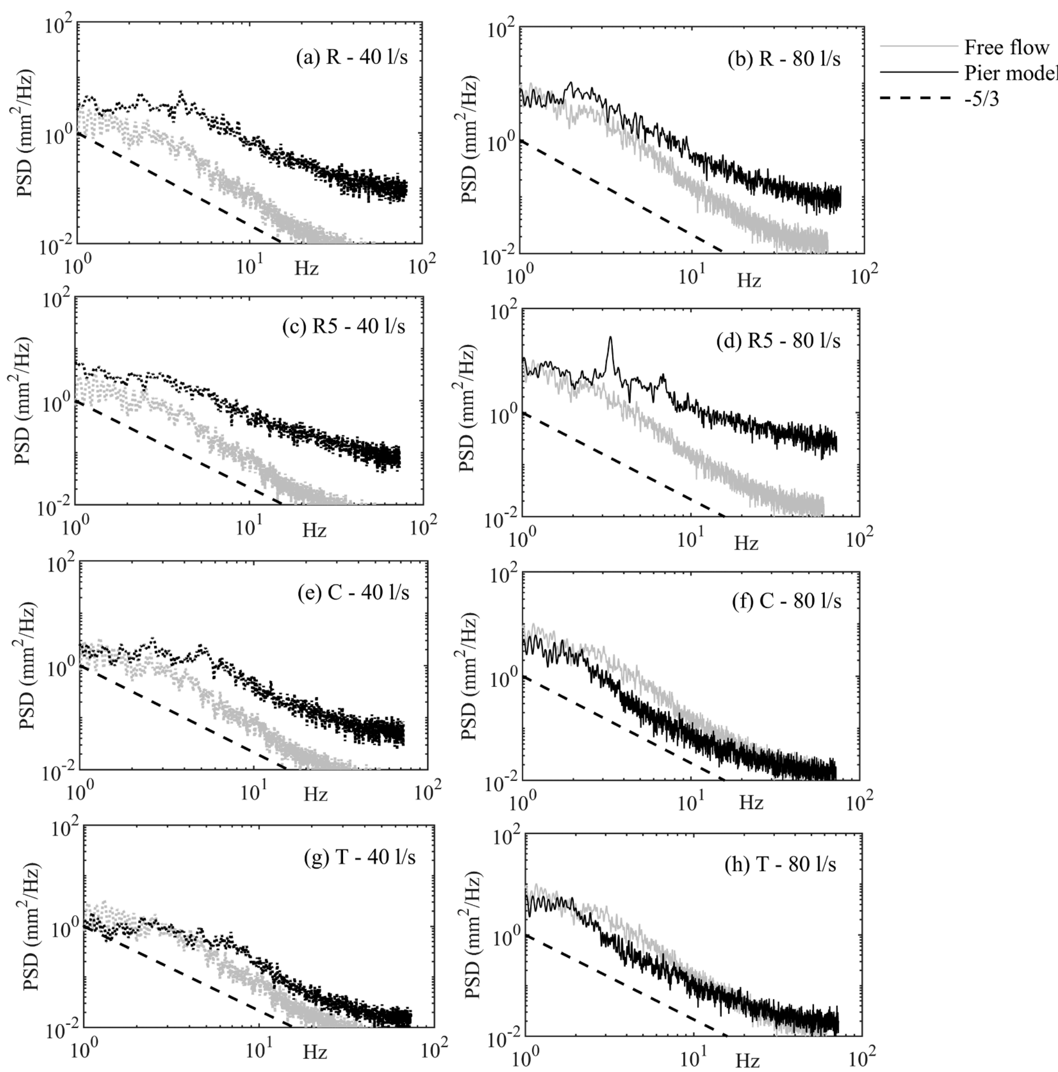

Fig. 5. Power spectral density of water surface oscillation for laboratory tested sections of pier models as indicated in Table 1 and for corresponding free flow conditions (i.e., 40 l/s and 80 l/s).

investigated during the conducted laboratory campaigns. For example, time correlations for Configuration R5 (rectangle 5 cm, flow facing width rectangular prism) and high flow condition ($Q = 80$ L/s) are reported in Fig. 6. Turbulent coherent structures were observed for all probes. Pier UVP (Fig. 6a) gave higher correlation values (close to 0.02) along almost the entire profiled range and within 0.05 s time lag. This corresponded to the large eddies trapped near the prism. This turbulent structure appeared further downstream: similar correlation values (close to 0.02) were observed for down looking UVPs (Fig. 6c, d and e). These highest values correspond to the main turbulent structure: the horseshoe vortex shape at prism wake. In addition to this main structure, additional relatively high values of correlation (close to 0.01) were observed at larger and equally spaced time lags (0.15 s, 0.30 s, 0.45 s). These relative peaks are particularly clear for UVP_{wk5} and UVP_{wk10} (Fig. 6c and d) although they can be argued for all probes. These reflect periodical passages of turbulence eddies through the obstacle wake, i.e., vortex shedding.

A more comprehensive comparison of time correlations is given in Fig. 7 where peaks and their corresponding time lags can be appreciated for the assessed time correlation averages along beams. Typical inverse relation between correlation and time lag was observed for all tests and probes that simply gave the expected coherence depletion for increasing time lag. This distribution depended on the pier section and probe position which reflected the changing features of turbulence structures, namely UVP_p (continuous lines in Fig. 7a and b) registered poorly sorted time lags for semicircular and triangular sections. This downstream oriented probe was sensitive to velocity oscillations along the flow directions. On the contrary, the UVP_b (dashed lines in Fig. 7a and Fig. 7b) was sensitive to vertical velocity oscillation which resulted in sharper distributions within 0.1 s time lag. These misalignments among vertical and flow directions bore out turbulent structure anisotropy that is to be related to pier shape and corresponding structure of boundary layer separation [12].

3.3. Turbulence oscillations and uncertainty

Results from power spectral density and time correlation were subjected to strong variations which depended on specific positions and tests for which turbulence measurement were conducted. For example, the integral scales values varied from 0.02 to 0.2 s. Shorter integral scales mostly combined with (i) higher values of frequency corresponding to PSD peaks and (ii) larger variation coefficients (i.e., standard deviation divided by the mean value) of velocity time-series at single cells (Fig. 8a and b). The same figures also reflect uncertainty of turbulent velocities: variation coefficient spanned two orders of magnitudes from 1 to 100 and PSD peaks were not univocally detected. In fact, aiming at statistical validation velocity measurement were repeated 32,800 times in each position for each given steady condition. This corresponded to about 3 to 4 min long and repeatable recordings of velocity time series.

Similarly, Fig. 4e shows PSD dispersion which can be related with its uncertainty. Values from 6 min time series at single cells define 95 % confidence levels bounding within about one order of magnitude the depth averaged power density, although the overall distribution remains similar (i.e., $-5/3$ power).

More intense and fast oscillating coherent patterns (i.e., larger uncertainty) were observed for the low flow condition that is particularly evident by isolating results from UVP_p and UVP_b (Fig. 9a). These also depended on the tested prism section and UVP probe deployment which bore out the anisotropic feature of observed turbulence structures.

For example, the low flow condition gave rise to shorter integral scale and higher variation coefficient at the bottom UVP than for the pier UVP (Fig. 9a) indicating more intense and fast oscillating patterns in the vertical direction rather than in the flow direction.

Furthermore, UVP_b resulted in shorter integral scale and larger variation coefficient for the low flow condition. This indicated an effect of water surface position on turbulent coherent structures. Eddies development along the vertical direction was bounded by water surface

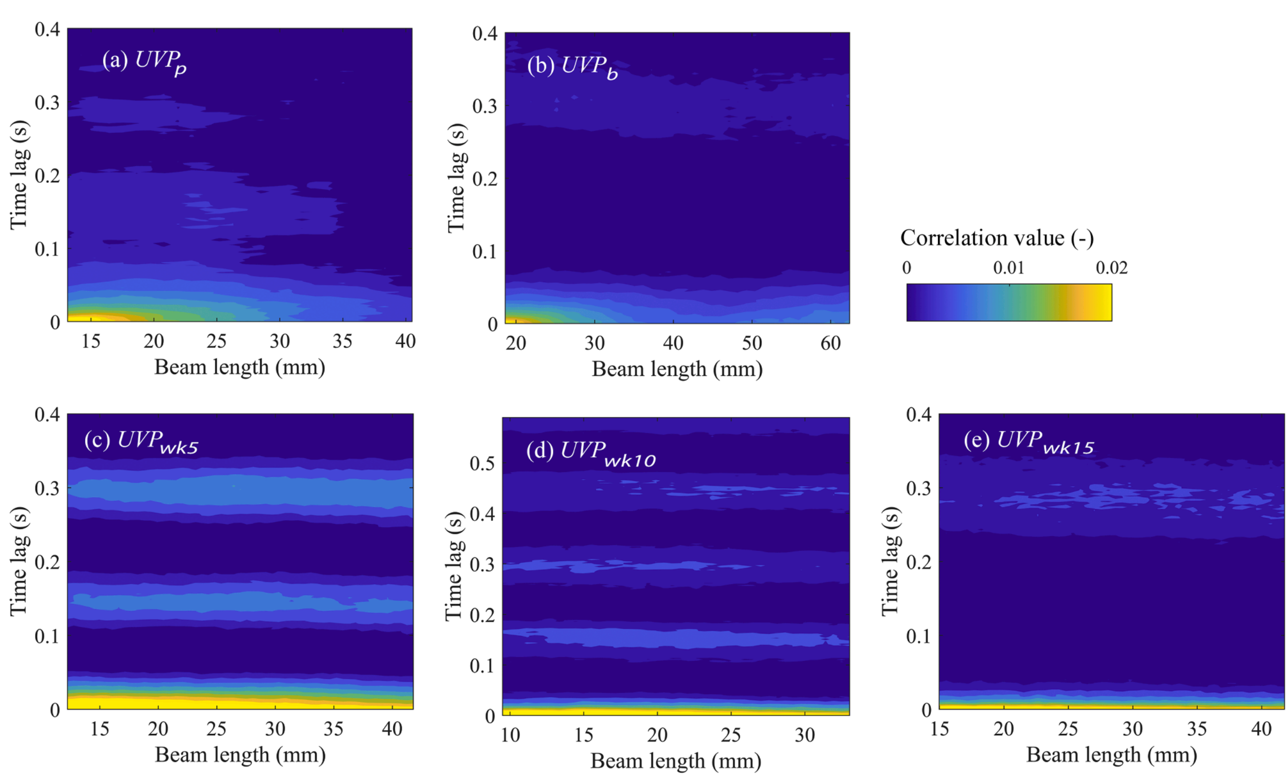

Fig. 6. Time correlations for R5 model pier and high flow condition (80 l/s): (a) Pier UVP, (b) UVP from the bottom, (c) 5 cm, (d) 10 cm and (e) 15 cm downstream spaced UVPs at pier wake as indicated in Fig. 2a.

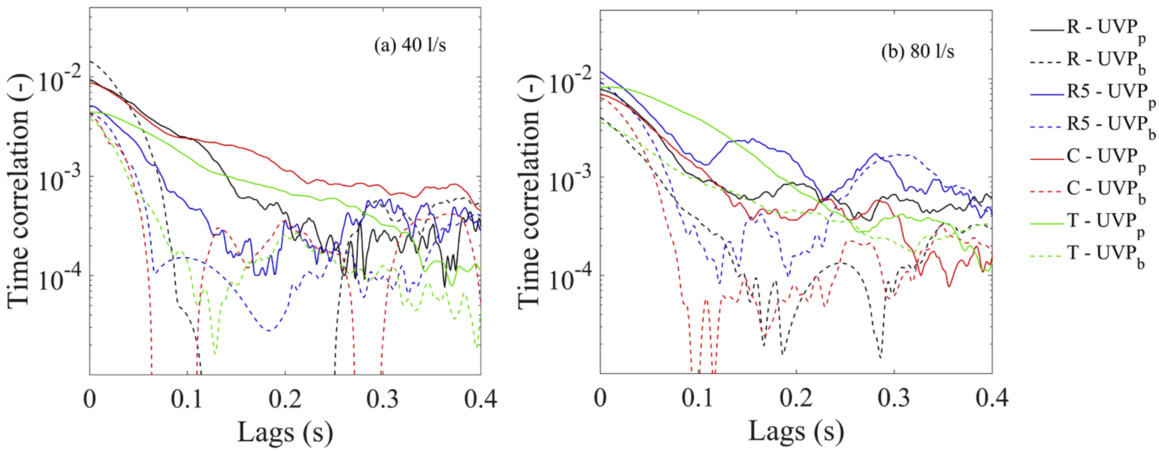

Fig. 7. Time correlations averaged along acoustic beams for tested pier sections as indicted in Table 1 and from pier UVP (solid lines) and UVP at bottom (dashed lines): (a) low and (b) high flow conditions.

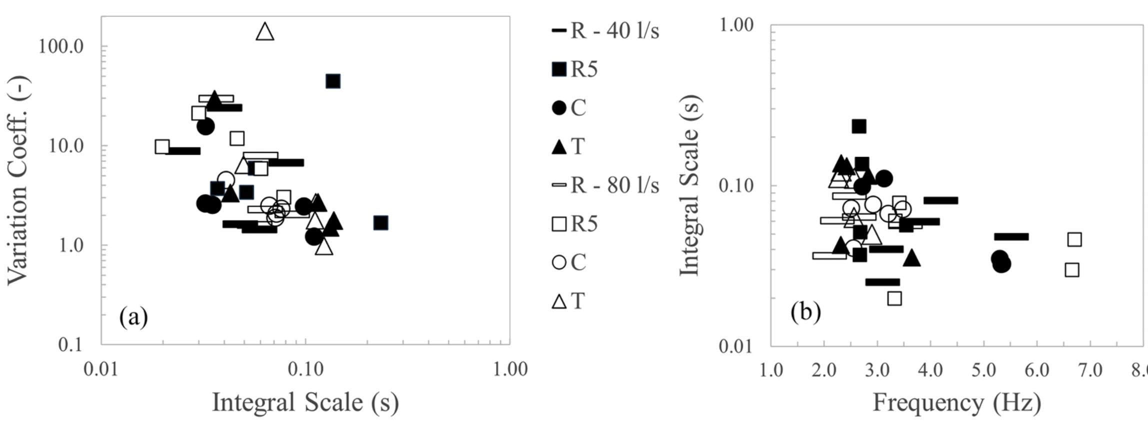

Fig. 8. (a) Integral scale vs. variation coefficient and (b) frequency corresponding to PSD peak vs. integral scale for all probes (not indicated), different pier sections as indicated in Table 1 and two flow conditions.

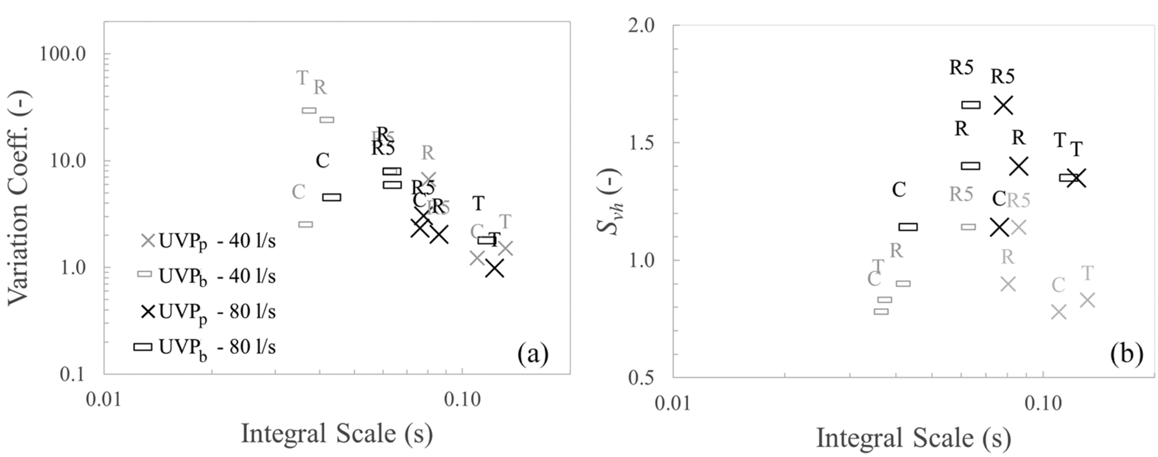

Fig. 9. (a) Integral scale vs. variation coefficient and (b) integral scale vs. dy/D (i.e., S_{vh} dimensionless parameter) for pier UVP and bottom UVP, different pier models as indicated in Table 1 and two flow conditions.

configuration which in turn depended on the flume section narrowing and consequent energy dissipation ascribable to tested piers. Thus, for example, rectangular sections produced larger water level drop, *dy*, that was especially the case for higher flow passage blockage. This larger drop was associated with observed higher levels (namely: the backwater effect) which yield additional room to coherent structure oscillation along the vertical direction, i. e., larger size eddies characterized with longer inertial scale and lower amplitude of velocity oscillating patterns.

As an additional consequence the observed frequency by UVP_b corresponding to PSD peaks decreased from the interval 3–6 Hz to the interval 2–4 Hz when passing from low to high flow condition, whereas they remained mostly unchanged within the range of 2 Hz to 4 Hz at the pier UVP that corroborated the finding of larger size and slower oscillating eddies in the vertical direction for higher water levels.

3.4. The impact of pier geometry on turbulence behavior

The triangular pier appeared with longer integral scale and smaller variation coefficient values for the UVP_p and for both flow conditions (Fig. 9a) when compared to semicircular and rectangular sections. The UVP_b was sensitive to eddies oscillation in the flow direction. The variation in integral scale suggests a horizontal contraction of turbulent eddies in the vicinity of semicircular and rectangular pier sections. This behavior is consistent with the abrupt separation of the boundary layer induced by normal (90°) impinging flow, which causes significant streamline deflection around the pier. Conversely, the streamlined geometry of the triangular pier facilitates a more gradual boundary layer detachment, enabling a smoother transition from the frontal region to the wake and resulting in more elongated downstream streamlines along the lateral sides of the pier. Bottom UVP exhibited a similar pattern although triangular and semicylinder piers appear more scattered (Fig. 9a) that might reflect coherent structures anisotropy [12].

Small differences were observed between rectangular piers having different sizes that indicated almost negligible scaling effect when passing from 5 cm to 10 cm size.

4. Discussion

Power Spectrum Density pattern observed at the wake of vertical piers appeared similar although scaled when passing from model to the Po River prototype (Fig. 4). This scaling is obviously related to the different lengths and flow conditions of the investigated processes which finally fixed the oscillating frequency of the observed turbulence structures. Aiming at characterizing those eddies and their generation under controlled conditions in laboratory environment, dimensionless parameters must be fixed [11]. Reynolds, Strouhal and Froude parameters appeared to be relevant in this case (Eqs. (1.1), 1.2 and 1.3) that might be reduced to the two latter by considering the existing parameterizations of Strouhal to Reynolds number for cylindric piers (e.g., [40]).

Turbulence coherent anisotropic structures were observed at laboratory scale that depended on the S_{vh} dimensionless parameter to a certain degree (Fig. 9b). This relation was further investigated at the prototype scale.

Following the Vaschy-Buckingham theorem. a rigorous dimensional analysis was produced. Relevant variables describing the investigated process were fixed: the acceleration due to gravity g, the geometrical parameters dy and D, the flow parameters U and h, most relevant turbulence features which are squared velocity fluctuations u'^2 and the frequency of flow vortex shedding f. These totalize seven parameters. The dimensional analysis gives three independent physical quantities corresponding to length, mass and time units which mean four non-dimensional groups (i.e., seven minus three). These correspond to the non-dimensional geometrical parameter, $S_{vh} = dy/D$. the Strouhal and Froude numbers (Eqs. (1.2) and 1.3) and a pier resistance coefficient ($C_r = u'^2/U^2$) which relates velocity fluctuation to mean flow velocity where the former is proportional to energy dissipation. This theoretically support an existing relationship among non-dimensional groups:

$$S_{vh} = S_{vh}(St, Fr, C_r) \tag{4.1}$$

that was experimentally investigated.

It's worth noting that fluid viscosity was not considered by this analysis that substantiated the use of investigated relationship across scales and flow regimes. This is valid for prevailing inertial over viscous forces (i.e., high values of the Reynolds number).

Indeed, The Vaschy-Buckingham theorem provides dimensionless groups of variables involved in the investigated process although the actual combinations are arbitrary and mostly fixed by historical reasons rather than rigorous mathematical procedure. Furthermore, the actual relationship (Eq. (4.1)) is not provided.

In fact, for example, a dimensionless parameter remains non-dimensional by multiplying it by other dimensionless parameters. In this case the non-dimensional variable, S_{vh}, may be expressed by combining Strouhal and Froude numbers as follows:

$$S_{vh} = \frac{dy}{D} = \frac{Fr^2}{St} = \frac{U^2}{gh}\frac{U}{fD} \tag{4.2}$$

where the Strouhal length scale was consistently fixed to the pier width D.

Aiming at expressing energy dissipation that is represented by the water level drop, the relevant scale of flow velocity U^2 was herein replaced with the squared velocity fluctuations u'^2 of turbulent coherent structures divided by C_r which yields

$$S_{vh} = \frac{dy}{D} = \frac{Fr^2}{St} = \frac{1}{C_r}\frac{u'^2}{gh}\frac{U}{fD} = \frac{1}{C_r}\frac{PSD}{gh}\frac{U}{D} = \frac{PSD}{C_r}\frac{Fr^2}{\varepsilon} \tag{4.3}$$

Where $PSD = u'^2/f$ has the form of a power spectral density and $\varepsilon = UD$ has the form of a turbulent viscosity representing the horizontal diffusion in the wake which is triggered by the pier width.

The relationship among non-dimensional parameters (Eq. (4.1)) and further elaborated as expressed by Eq. (4.3), was experimentally investigated and resulted close to predictable and quasi linear relationship in Fig. 10 by assuming unit resistance coefficient C_r. In fact, deviations from linear behavior arose for the high flow condition tested at laboratory scale. In this case, and for 10 cm prism sections, the observed water level drops were higher than predicted by a linear relationship (that is for fixed C_r). In fact, the backwater effect was exacerbated by combining greater discharge with larger obstacles. Simply substituting flow squared velocity U^2 with the squared oscillating velocity u'^2 in Eq. (4.3), neglected the effect of obstacle shape on energy dissipation that might be considered by investigating the resistance coefficient change due to the specific shapes of pier section. However, for sake of simplicity, and targeting fidelity while scaling coherent turbulent structures around a vertical pier, these results show that the S_{vh} geometrical parameter should be considered.

4.1. Application to a historical case: a speculative interpretation of Leonardo da Vinci's visual acuity

A known application of the theory of similarity was made by G.I. Taylor to estimate the yield of the Trinity nuclear test based on the

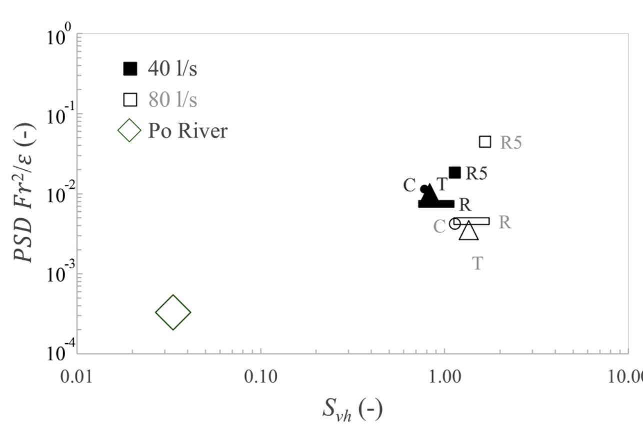

Fig. 10. (a) S_{vh} geometrical dimensionless parameter, dy/D, and corresponding features of observed turbulence structures as summarized from Equation 1.6 for the pier bridge at Po River (diamond mark) and for different configurations of pier models as reported in Table 1.

images published in printed media with the respective time stamp and spatial scale [41]. This often-cited example drove this discussion about the possibility of applying observed criteria of similarity to the drawings of Leonardo da Vinci (Fig. 11a).

Leonardo da Vinci was born in Vinci, Italy, in 1452 and died in Amboise, France in 1519. He was the epitome of the Renaissance man: artist, scientist and engineer [42]. Leonardo's genius covered a wide range of disciplines which he documented in his wide body of artistic works and his series of Codices. Among those, in Codex Atlanticus [43] the word turbulence was first mentioned [44]. Leonardo's interest in turbulent water flows is reflected by his extensive body of work on the topic [45]. In his drawings of water flows it is possible to identify different types of flows such as the flow around blunt bodies, floods and impinging jets. In his Studies of Water, Leonardo (1510) [46] writes: "Observe the motion of the surface of the water, which resembles that of hair, which has two motions, one of which depends on the weight of the hair, the other on the direction of the curls; thus the water forms turning eddies, one of which follows the impetus of the main course while the other follows that of incidence and re-flection." It is not difficult to relate this sentence with the famous poem by Richardson [47] "Big whirls have little whirls / that feed on their velocity, / and little whirls have lesser whirls / and so on to viscosity."

Leonardo's drawings depict water turbulent flow by representing vortices and trajectories which recall the theoretical and analytical studies of turbulence dynamics developed centuries later [48]. Namely the representation of turbulent energy cascade from large eddies where this is produced up to its dissipation occurring at the Kolmogorov micro scale. Kolmogorov's pioneering work [49] investigating eddies wave-number spectrum in the inertial subrange which quantifies energy transfer from large to microscale eddies is somehow anticipated in Leonardo's drawings of water turbulent flows although no quantitative information is provided, namely about the physical dimensions of the setup.

Turbulent features such as wake flow downstream of a vertical single pier depend on flow conditions, obstacle size and shape [8,9,12,50] that, indeed, are not documented in Leonardo's drawings. Colagrossi et al. [44] posed a pertinent question: "What was actually represented by Leonardo (size, conditions, flow characteristics…)?" Since, Leonardo didn't provide any scale in his notes nor elsewhere in his studies. Colagrossi et al. [44] suggested that the lack of knowledge about the metrics in his drawings requires educated guesses about the geometry and flow conditions to eventually investigate the physics behind his observation.

Strouhal and Froude dimensionless parameters would characterize the oscillating turbulence pattern observed and depicted by Leonardo da Vinci. Unfortunately, from his artistic rendition, only S_{vh} dimensionless parameter, might be estimated from vertical to horizontal scales of his drawing.

The previous analysis of the flow around models pier and Po River pier, corroborated the hypothesis that power spectral density of oscillating turbulence patterns can be characterized quantitatively with S_{vh} dimensionless parameter, and this argument can be used to speculate about the flow around the obstacle depicted by Leonardo.

An analysis of Leonardo's drawing (Fig. 11a) was performed using image processing to account for the perspective distortion [51] (Fig. 11c-e). This procedure made possible to estimate the ratio between the represented dimensions, namely the ratio between water level drop across the obstacle and its width facing the flow, S_{vh}, was estimated to be in the order of 10°.

Turbulent horseshoe wake as depicted by Leonardo appeared similar to the horseshoe wake in lab tests (Fig. 11b). Furthermore, passage close to critical condition appears evident in his depicting that bound educated guessing regarding the actual scale of Leonard's drawing. In fact, Froude dimensionless parameter switching across the pier, as it occurred for laboratory tests (see Table 1), further simplifies the proposed relationship in Equation 1.6. In this case, the turbulent horizontal viscosity ε is the only parameter to be defined to eventually infer the PSD order of magnitude by knowing S_{vh}.

It's worth noting that turbulent horizontal viscosity, ε, was 10^{-2} m^2/s as an order of magnitude for laboratory tests and it was two orders of magnitudes higher at the Po River. Furthermore, S_{vh} was close to 1 and 10^{-2}, respectively (Fig. 10). Therefore, Leonardo's observation of turbulent horseshoe wake was likely focusing on similar coherent structures such as those reconstructed in the hydraulic laboratory.

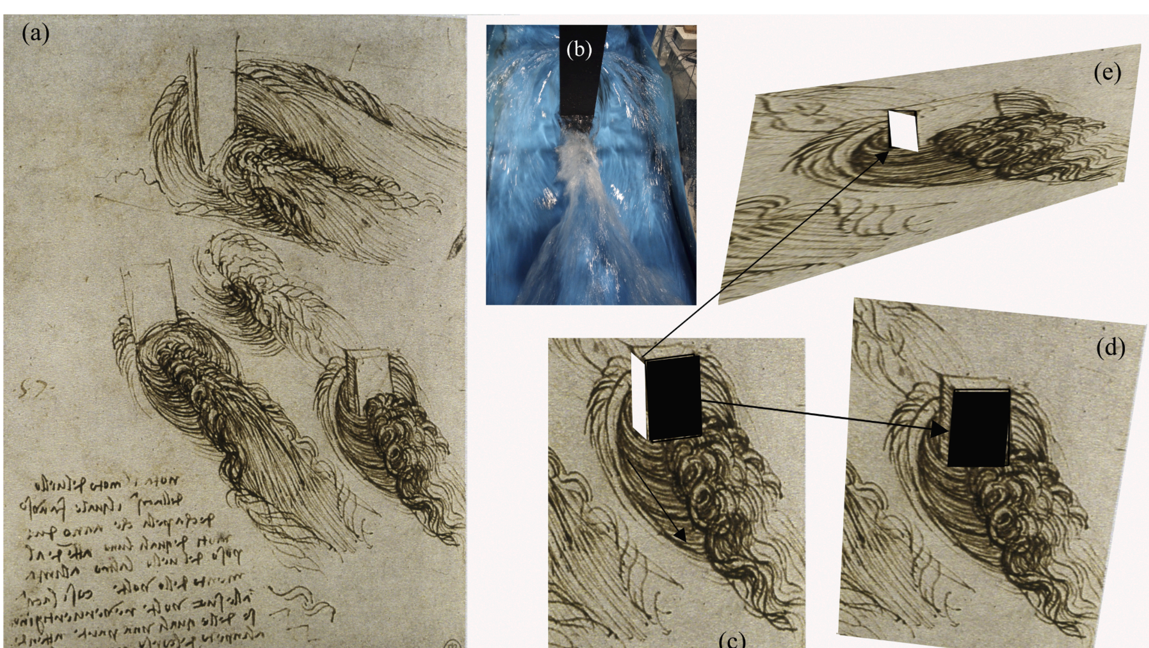

Fig. 11. (a) Leonardo da Vinci's turbulent flow downstream of an isolated pier in Leonardo da Vinci's Studies of water (c.1510–12). Sheet RCIN 912579r. Royal Collection Trust Copyright Her Majesty Queen Elizabeth II 2021. (b) Horseshoe vortex at laboratory experiment to be compared to Leonardo's drawing (c) Identification of the pier sides to be corrected for perspective; (d) and (e).

This alignment between his drawings and the analytical description of turbulence oscillations raised questions about his means of observing and eventually fix on paper those oscillating patterns, namely, Leonardo's visual acuity. In fact, a well consolidated rule in the experimental approach dealing with variable and oscillating physical process, such as turbulent flow, is to apply a much larger (e.g., 10–100 times) acquisition frequency than the expected rate of variation (i.e., the oscillating frequency) to eventually document those dynamics. This is mathematically expressed by Nyquist–Shannon sampling theorem which fixes the lower limit of sampling rate equal to two times the observed frequency for unbiased acquisition [52,53].

It is then possible to infer about Leonardo's visual acuity. Integral scales bounding the inertial subrange, where coherent structures develop, ranged from 0.04 s to 0.1 s for probes deployed within the horseshoe wake (UVP_b and UVP_p in Fig. 9a). The acquisition and depicting of these oscillating patterns would require from 2 to 10 times larger sampling rate than the expected frequency content, where the lower limit represents the Nyquist–Shannon minimal threshold and 10 times may represent a good instrument to characterize the expected oscillations with such details. Therefore, from the conducted experimental campaign it is possible to surmise that Leonardo's visual time resolution was at least about 100 Hz well in advance of theoretical studies and instrumentation development.

5. Conclusions

Conducted experimental campaign at two well-spaced scales, i.e., a model in a hydraulic flume and the prototype in the Po River, showed the importance of S_{vh}, vertical to horizontal geometrical scaling, when reproducing turbulent coherent structures associated with the horseshoe wake around isolated piers.

The relation between flow features and S_{vh} was experimentally investigated. Simple metrics of turbulence oscillations such as the frequency power spectral density of velocity single components and corresponding time correlations were inferred by means of ultrasound Doppler techniques. Resulting patterns were related to flow conditions parameters (Reynolds, Froude and Strouhal numbers).

The S_{vh} parameter well represented the scaling of the turbulence power spectral density with horizontal turbulent viscosity due to pier width, provided that the Froude dimensionless parameter remain unchanged. Therefore, aiming at reproducing prototype power spectral density while scaling pier width size in a laboratory test, the Froude criteria should be paired by the scaling of turbulence features. Power spectral density resulted proportional to horizontal turbulent viscosity ($U \times D$).

This finding bounded an educated guess about the scale of Leonardo da Vinci drawing and gave hints on his visual acuity. Rectangular, semicircular and triangular sections of prism piers which were tested at model scale well reproduced the S_{vh} geometrical parameter estimated for Leonard's drawing. Those experiments resulted in turbulence fluctuations developing within the inertial subrange spanning from 0.04 s to 0.1 s in terms of integral scale. Leonardo da Vinci's investigation and drawing of turbulent oscillations would have required a visual time resolution of about 100 Hz.

CRediT authorship contribution statement

Massimo Guerrero: Writing – review & editing, Writing – original draft, Visualization, Validation, Supervision, Software, Resources, Methodology, Investigation, Funding acquisition, Formal analysis, Data curation, Conceptualization. **Rui Aleixo:** Writing – review & editing, Visualization, Validation, Supervision, Software, Resources, Project administration, Methodology, Investigation, Funding acquisition, Formal analysis, Data curation, Conceptualization. **Leonardo Schippa:** Writing – review & editing, Resources, Methodology, Investigation, Funding acquisition, Formal analysis, Data curation.

Declaration of competing interest

The authors declare the following financial interests/personal relationships which may be considered as potential competing interests: Rui Aleixo reports financial support was provided by Richard Lounsbery Foundation. If there are other authors, they declare that they have no known competing financial interests or personal relationships that could have appeared to influence the work reported in this paper.

Acknowledgment

The authors thank the Richard Lounsbery Foundation, USA, (www.rlounsbery.org) for the funding provided in the scope of Leonardo da Vinci DNA Project. The authors thank the Po River Agency, namely AIPo- Agenzia Interregionale per il fiume Po (https://www.agenziapo.it/), for supporting river survey activities with dedicated crew, means and instrumentation to field work at Pontelagoscuro bridge (Ferrara - Italy).

Data availability

Data will be made available on request.

References

[1] Y.A. Cengel, J.M. Cimbala, Approximate solutions of the Navier-stokes equation. Fluid Mechanics: Fundamentals and Applications, 4th edition, Mc Graw-Hill, New York, 2018. ISBN:1259921905.

[2] C.R. Ethier, D.A. Steinman, Exact fully 3D Navier–Stokes solutions for benchmarking, Int. J. Numer Methods Fluids 19 (5) (1994) 369–375, https://doi.org/10.1002/fld.1650190502.

[3] F. White, Viscous Fluid Flow, 2nd edition, McGraw Hill, New York, 1991. ISBN:0-07-069712-4.

[4] D. McLean, Continuum fluid mechanics and the navier-stokes equations. Understanding Aerodynamics: Arguing from the Real Physics, John Wiley & Sons, West Sussex, United Kingdom., 2012, pp. 13–78, https://doi.org/10.1002/9781118454190. ISBN:9781119967514.

[5] M. Guerrero, F. Latosinski, M. Nones, R.N. Szupiany, M. Re, M.G.A. Gaeta, Sediment fluxes investigation for the 2-D modelling of large river morphodynamics, Adv. Water Resour. 81 (2015) 186–198, https://doi.org/10.1016/j.advwatres.2015.01.017.

[6] D. Termini, V. Sammartano, Morphodynamic processes downstream of man-made structural interventions: experimental investigation of the role of turbulent flow structures in the prediction of scour downstream of a rigid bed, Phys. Chem. Earth 49 (2012) 18–31, https://doi.org/10.1016/j.pce.2011.12.006.

[7] A. Anand, M. Beg, Local scour at group of bridge piers founded in gravel bed in staggered arrangement, Results Eng. 23 (2024) 1–10, https://doi.org/10.1016/j.rineng.2024.102608, 102608.

[8] Q. Chen, D. Zhang, Z. Wang, H. Zhang, Q. Zhong, Experimental study on the characteristics of near-wall flow and instantaneous wall shear stress in front of wall-mounted cylinders, Experiment. Thermal and Fluid Sci. 163 (2025) 111424, https://doi.org/10.1016/j.expthermflusci.2025.111424.

[9] S. Dey, D. Swargiary, S. Sarkar, H. Fang, R. Gaudio, Self-similarity in turbulent wall-wake flow downstream of a wall-mounted vertical cylinder, J. Hydraul. Eng. 144 (6) (2018) 04018023, https://doi.org/10.1061/(ASCE)HY.1943-7900.00014.

[10] N. Safaripour, M. Vaghefi, A. Mahmoudi, Scour variations around pier groups at a sharp bend with triad vanes, Results in Eng. 23 (2024) 1–12, https://doi.org/10.1016/j.rineng.2024.102617, 102617.

[11] V. Heller, Scale effects in physical hydraulic engineering models, J. Hydraul. Res. 49 (3) (2011) 293–306, https://doi.org/10.1080/00221686.2011.578914.

[12] B. Dargahi, The turbulent flow field around a circular cylinder, Exp. Fluids 8 (1–2) (1989) 1–12, https://doi.org/10.1007/BF00203058.

[13] L.I. Sedov, Similarity and Dimensional Methods in Mechanics, 10thedition, CRC Press, 1993.

[14] M.S. Yalin, Theory of Hydraulic Models, Macmillan Civil Engineering Hydraulics, Palgrave, London, 1971, https://doi.org/10.1007/9781-349-00245-02.

[15] O. Reynolds, An experimental investigation of the circumstances which determine whether the motion of water shall be direct or sinuous, and of the law of resistance in parallel channels, Proceed. Royal Society of London 35 (224–226) (1883) 84–99, https://doi.org/10.1098/rspl.1883.0018.

[16] E. Buckingham, On physically similar systems; illustrations of the use of dimensional equations, Phys. Rev. 4 (4) (1914) 345.

[17] A. Vaschy, Sur les lois de similitude en physique, Annales télégra-phiques 19 (1892) 25–28 (in French).

[18] M. Guerrero, A. Lamberti, Loose-bed models for river structure design: two example studies on river Po, in: *Proceedings of the International Conference on Fluvial Hydraulics - River Flow 2006*, Lisbon, 2, 2006, pp. 1915–1922.

[19] H. Rouse, S. Ince, History of hydraulics. Iowa Inst. of Hydraulic Research, State University of Iowa, 1957.
[20] Y. Takeda, Velocity profile measurement by ultrasonic doppler method, Experiment. Thermal and Fluid Sci. 10 (4) (1995) 444–453, https://doi.org/10.1016/0894-1777(94)00124-Q.
[21] Y. Takeda, Ultrasonic Doppler Velocity Profiler for Fluid Flow, Springer, 2012. ISBN:978-4-431-54025-0.
[22] L. Bressan, M. Guerrero, A. Antonini, V. Petruzzelli, R. Archetti, A. Lamberti, S. Tinti, A laboratory experiment on the incipient motion of boulders by high-energy coastal flows, Earth Surface Processes and Landforms 43 (14) (2018) 2935–2947, https://doi.org/10.1002/esp.4461.
[23] S. Conevski, R. Aleixo, M. Guerrero, N. Ruther, Bedload velocity and backscattering strength from mobile sediment bed: a laboratory investigation comparing bistatic versus monostatic acoustic configuration, Water-MDPI 12 (12) (2020) 3318, https://doi.org/10.3390/w12123318.
[24] G. De Cesare, J.-L. Boillat, Flow velocity measurements using ultrasound doppler method - 10 years experience in hydraulic modeling, in: Proceedings of 5th international symposium on ultrasonic doppler methods for fluid mechanics and fluid engineering ISUD, ETH Zurich, Switzerland, 2006, pp. 113–116.
[25] D. Dufour, F.X. Tanner, K.A. Feigl, E.J. Windhab, Investigation of the dispersing characteristics of antral contraction wave flow in a simplified model of the distal stomach, Phys. Fluids 33 (8) (2021), https://doi.org/10.1063/5.0053996 art. no. 083101.
[26] DOP, Model 2125, User's manual (software 2.01, Revision 1.0), Signal Processing S.A., Lausanne, Switzerland, 2000.
[27] L.E. Kinsler, A.R. Frey, A.B. Coppens, J.V. Sanders, Fundamentals of Acoustics, 4th edition, Wiley, 2000. ISBN 0471847895.
[28] D.G. Goring, V.I. Nikora, Despiking acoustic Doppler velocimeter data, J. Hydraul. Eng. 128 (1) (2002) 117–126, https://doi.org/10.1061/(ASCE)0733-9429(2002)128:1(117.
[29] M.G. Gaeta, M. Guerrero, S.M. Formentin, G. Palma, B. Zanuttigh, Non-intrusive measurements of wave-induced flow over dikes by means of a combined ultrasound doppler velocimetry and videography, Water-MDPI 12 (11) (2020) 3053, https://doi.org/10.3390/w12113053.
[30] P.A. Davidson, *Turbulence: An Introduction For Scientists and Engineers*,, 2nd edition, Oxford University Press, 2015, https://doi.org/10.1093/acprof:oso/9780198722588.001.0001. ISBN: 9780198722588.
[31] H. Tennekes, J.L. Lumley, A First Course in Turbulence, The MIT Press, 1972, https://doi.org/10.7551/mitpress/3014.001.0001. ISBN:9780262310901.
[32] J.M. Wallace, Space-time correlations in turbulent flow: a review, Theoret. Appl. Mechan. Lett. 4 (2014) 2, https://doi.org/10.1063/2.1402203. ISSN:2095-0349.
[33] S. Conevski, M. Guerrero, C.D. Rennie, N. Ruther, Towards an evaluation of bedload transport characteristics by using Doppler and backscatter outputs from ADCPs, J. Hydraul. Res. 59 (5) (2021) 703–723, https://doi.org/10.1080/00221686.2020.1818311.
[34] M. Guerrero, S. Conevski, I. Cavalieri, L. Schippa, N. Ruther, Influence of hydropower propellers on open-channel flow, J. Hydraul. Eng. 149 (11) (2023) 04023047, https://doi.org/10.1061/JHEND8.HYENG-13417.
[35] E.A. Nystrom, C.R. Rehmann, A.K. Oberg, Evaluation of mean velocity and turbulence measurements with ADCPs, J. Hydraul. Eng. 133 (12) (2007) 1310–1318, https://doi.org/10.1061/(ASCE)0733-9429.
[36] D.R. Parsons, P.R. Jackson, J.A. Czuba, F.L. Engel, B.L. Rhoads, K.A. Oberg, J. L. Best, D.S. Mueller, K.K. Johnson, J.D. Riley, Velocity mapping Toolbox (VMT): a processing and visualization suite for moving-vessel ADCP measurements, Earth Surf. Processes Landforms 38 (11) (2013) 1244–1260, https://doi.org/10.1002/esp.3367.
[37] RD Instruments, Acoustic Doppler current profiler principles of operation, A Practical Primer (2011). Accessed August 20, 2023, https://www.teledynemarine.com/en-us/support/SiteAssets/RDI/Manuals%20and%20Guides/General%20Interest/BBPRIME.pdf.
[38] B.H. Brumley, R.G. Cabrera, K.L. Deines, E.A. Terray, Performance of a broad-band acoustic Doppler current profiler, IEEE J. Oceanic Eng. 16 (1991) 402–407, https://doi.org/10.1109/48.90905.
[39] K. Blanckaert, U. Lemmin, Means of noise reduction in acoustic turbulence measurements, J. Hydraul. Res. 44 (1) (2006) 3–17, https://doi.org/10.1080/00221686.2006.9521657.
[40] J.H. Lienhard, *Synopsis of lift, drag, and vortex frequency data for rigid circular cylinders* (PDF). College of Engineering, Research Division (Report). Bulletin 300, Washington State University, Pullman, WA, 1966. Retrieved February 7, 2025.
[41] M.A.B Deakin, G.I. Taylor and the Trinity test, Int. J. Math. Educ. Sci. Technol. 42 (8) (2011) 1069–1079, https://doi.org/10.1080/0020739X.2011.562324.
[42] Vasari, G. (1568), *The lives of the most excellent painters, sculptors, and architects, Modern Library*; Reprint edition (February 14, 2006).
[43] Edited by Leonardo da Vinci (1478-1519), in: Augusto Marinoni (Ed.), Codex Atlanticus, Hoepli, 1975. Edited by.
[44] A. Colagrossi, S. Marrone, P.D. Colagrossi, P. Le Touzé, Da Vinci's observation of turbulence: a French-Italian study aiming at numerically reproducing the physics behind one of his drawings, 500 years later, Phys. Fluids 33 (11) (2021) 115122, https://doi.org/10.1063/5.0070984.
[45] Leonardo da Vinci (ca. 1508–1510), *Codex Leicester* [Manuscript]. Private collection, Bill Gates, Medina, WA.
[46] edited by Leonardo da Vinci, Studies of water, in: Martin Kemp (Ed.), Reproduced in Leonardo da Vinci: The Complete Drawings, Taschen, 1510, p. 2006. edited by.
[47] L.F. Richardson, Weather Prediction by Numerical Processes, Cambridge University Press, Boston, 1922, p. 66. ISBN:9780511618291.
[48] F. Capra, The Science of Leonardo: Inside the Mind of the Great Genius of the Renaissance, Doubleday, 2007. ISBN:978-0385513906.
[49] A.N. Kolmogorov, The local structure of turbulence in incompressible viscous fluid for very large reynolds numbers, Dokl. Akad. Nauk SSSR 30 (1941) 301–304.
[50] B.A. Vijayasree, T.I. Eldho, B.S. Mazumder, Turbulence statistics of flow causing scour around circular and oblong piers, J. of Hydraul. Res. 58 (4) (2020) 673–686, https://doi.org/10.1080/00221686.2019.1661292.
[51] M. Chan, Perspective control/correction. https://www.mathworks.com/matlabcentral/fileexchange/35531-perspective-control-correction, 2025. MATLAB Central File Exchange. Retrieved April 2, 2025.
[52] R.J. Marks, II, Introduction to Shannon Sampling and interpolation theory. Springer Texts in Electrical Engineering, Springer, 1991, https://doi.org/10.1007/978-1-4613-9708-3. ISBN 978-1-4613-9708-3.
[53] H. Nyquist, Certain Topics in Telegraph Transmission Theory, 47, AIEE, 1928, pp. 617–644, https://doi.org/10.1109/t-aiee.1928.5055024, 2Bibcode: 1928TAIEE..47..617NReprint as classic paper in: Proceedings of the IEEE, Vol. 90, No. 2, February 2002.